Revista Minelor – Mining Revue
ISSN-L 1220-2053 / ISSN 2247-8590
vol. 31, issue 3, pp. 9-27, selected paper from the First International EnviroMining Virtual Conference 2025

STUDY ON THE INFLUENCE OF IN-SITU STRESS LEVELS ON THE DAMAGE CHARACTERISTICS OF SURROUNDING ROCK DURING DRILL-AND-BLAST EXPANSION OF TBM PILOT TUNNELS

Qiaoyu GAO[1,4], *Peng YAN*[2*], *Stefano BONDUÀ*[3]

[1]Wuhan University, Wuhan, China, qiaoyugao@whu.edu.cn
[2]Wuhan University, Wuhan, China, pyanwhu@whu.edu.cn
[3]University of Bologna, Bologna, Italy, Stefano.bondua@unibo.it
[4]University of Bologna, Bologna, Italy, qiaoyu.gao@unibo.it

DOI: 10.2478/minrv-2025-0025
received – 18.01.2025 / revised – 10.02.2025
accepted – 17.02.2025 / published – 22.09.2025

Abstract: *The "Small-Diameter TBM Pilot Tunnel + Drill-and-Blast Expansion" method is a key excavation approach for long tunnels, combining the advantages of TBM and drill-and-blast methods to enable rapid and efficient construction. However, the understanding of surrounding rock damage caused by this method remains limited. This study combines field experiments and numerical simulations to analyze surrounding rock damage during drill-and-blast expansion and investigates the effects of in-situ stress factors, such as tunnel burial depth and lateral pressure coefficient. Results show that excavation advancement is closely linked to the ratio of advancement between full-face drill-and-blast and TBM methods. When both methods achieve double the advancement of full-face drill-and-blast, significant time-saving advantages are evident. Surrounding rock damage is positively correlated with burial depth, with deeper tunnels shifting failure modes from compressive-shear to tensile-shear composite failure, increasing tensile cracks. In shallow tunnels (burial depth < 450 m), drill-and-blast expansion reduces rock damage by approximately 10% compared to full-face drill-and-blast, but this effect weakens with depth. Lateral pressure coefficient impacts damage nonlinearly, with high values leading to extensive tensile cracks near sidewalls. Regression analysis reveals normalized contribution rates of 61.2% for burial depth and 38.8% for lateral pressure coefficient. These findings offer theoretical support for applying this method in long tunnel construction.*
Keywords: *Drilling and blasting expansion; TBM pilot in advance; Blast-induced damage; Tunnel depth; Pilot tunnel diameter; Sensitivity analysis*

1. Introduction

Drill-and-blast and Tunnel Boring Machine (TBM) methods are currently the two most commonly employed techniques for tunnel excavation. The selection of an appropriate excavation method primarily depends on the specific characteristics of the project and the geological conditions of the surrounding rock mass [1, 2]. The drill-and-blast method is characterized by its strong adaptability and construction flexibility; however, it is associated with slower excavation speeds, numerous operational steps, challenges in controlling over-excavation and under-excavation, and significant disturbance to the surrounding rock [3]. In contrast, the TBM method offers advantages such as high excavation speed and minimal disturbance to the rock mass. However, it has stringent requirements for geological conditions and is generally not recommended in poor geological zones, such as areas prone to rockbursts, water inflow, or karst development [4]. Furthermore, TBMs typically produce circular tunnel cross-sections. For large or extra-large cross-section traffic tunnels, using TBM excavation can result in significant space wastage and technical challenges. Currently, TBMs with diameters ranging from 3 to 6 meters are commonly used. As the excavation diameter increases, the efficiency of TBM tunneling decreases significantly [5–7]

* Corresponding author: Peng Yan, Prof. Wuhan University, Wuhan, China, contact details: 299 Bayi Road, Wuchang District, Wuhan, Hubei, China, pyanwhu@whu.edu.cn

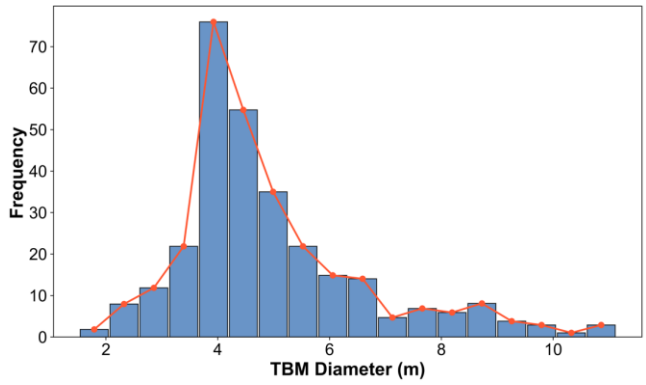

Fig. 1. Statistical chart of TBM diameter usage frequency

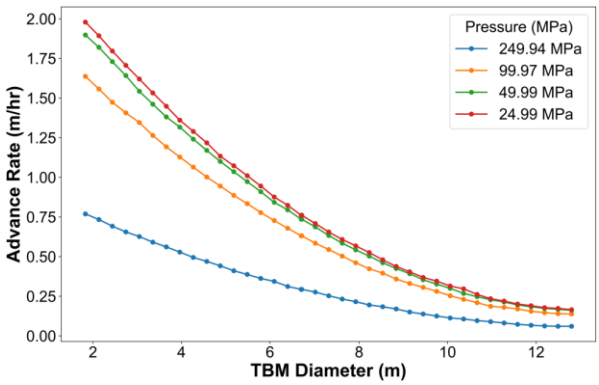

Fig. 2. Comparison of advance rate performance

The "Small-Diameter TBM Pilot Tunnel + Drill-and-Blast Enlargement" method is an important combined excavation approach in tunneling, leveraging the advantages of both the TBM and drill-and-blast methods [8, 9]. This approach is particularly suitable for constructing large cross-section tunnels under challenging geological conditions, such as fault zones, collapses, or large deformation in weak rock masses. The method involves initially excavating a pilot tunnel with a small-diameter TBM, followed by enlarging the tunnel to the designed profile using the drill-and-blast technique. As early as the 1980s, Italy pioneered the use of TBMs with diameters of 3.5–5 m to design and construct large-scale highway, railway, metro, and hydraulic tunnels. According to incomplete statistics, over 100 large cross-section tunnels worldwide have been constructed using this method since 1982. In Asia, countries such as Japan and South Korea have also implemented numerous projects employing the TBM pilot tunnel and drill-and-blast enlargement method. Table 1 summarizes representative tunnel projects constructed using the small-diameter TBM pilot tunnel and enlargement approach [10, 11].

Table 1. Tunnel projects using the small-diameter TBM pilot tunnel and enlargement method

Tunnel Name	Country	Diameter of pilot tunnel (m)	Tunnel cross-section size (m^2)	Length (km)	Year of Completion
Strada Statale 36	Italy	3.5	90		1987
Frasnadello Tunnel and Antea Tunnel	Italy	3.9	110	2.4	1996-1997
New Tomei-Meishin Expressway	Japan	5	190		Before 2003
Mappo-Morettina Road Tunnel	Switzerland	4.5	91.61	5.518	1996
Mount Macdonald Tunnel	Canada	6.7		14.66	1988
Num-sum	Korea	4.5		1.03	1991

The "Small-Diameter TBM Pilot Tunnel + Drill-and-Blast Enlargement" method provides a free surface for subsequent drill-and-blast operations, effectively reducing blasting-induced vibration effects. Theoretically, this excavation approach can increase the single-cycle advance rate of the drill-and-blast method, thereby significantly improving blasting efficiency. Additionally, the pilot tunnel facilitates the investigation of geological conditions ahead of the excavation, enhancing the overall safety of tunnel construction. However, the increased blasting advance rate implies a larger charge per cycle, which may result in greater blasting- induced damage to the remaining rock mass. In general, transient unloading effects during blasting play a significant role in causing rock mass damage, which is largely influenced by the in-situ stress environment. Whether the excavation of the pilot tunnel affects these transient unloading effects remains an open question requiring further investigation. This study aims to address these issues by combining field experiments with discrete element numerical simulations to analyze the impact of this method on rock mass stability and excavation performance. By focusing on micro-crack propagation and macroscopic failure mechanisms, this research seeks to provide scientific evidence and theoretical support for the application of the "Small-Diameter TBM Pilot Tunnel + Drill-and-Blast Enlargement" method in engineering projects.

2. Field experiments

2.1. Overview of field experiments sites

The field experiments were conducted at a pumped storage power station in Zhejiang Province, China, with a total installed capacity of 1200 MW, consisting of four units, each with a capacity of 300 MW. The project comprises key structures such as an upper reservoir, a lower reservoir, a water conveyance system, an underground powerhouse complex, and a surface switchyard. The access tunnel to the underground powerhouse, approximately 1913.516 km in length, serves as the primary construction and transportation passage for the powerhouse excavation during the construction phase. In the operational phase, it functions as a critical passage for traffic, ventilation, and emergency evacuation, making it a vital component of the underground excavation process. To evaluate the applicability of the "Small-Diameter TBM Pilot Tunnel + Drill-and-Blast Enlargement" method, a combined construction approach was implemented in the access tunnel, involving a small-diameter TBM (ϕ3.53 m) for pilot excavation followed by drill-and-blast enlargement. Other caverns in the project were excavated using the full-face drill-and-blast method. For comparison, the 2# construction branch tunnel, which is located near the access tunnel and shares similar surrounding rock properties, was selected. The 2# branch tunnel was entirely excavated using the full-face drill-and-blast method. The location and excavation details of the access tunnel are shown in Fig. 3.

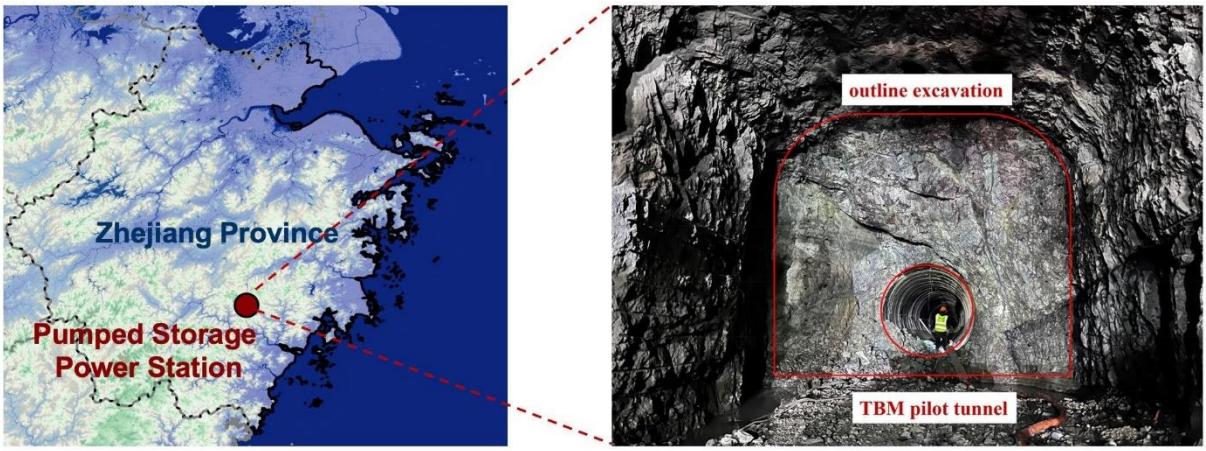

Fig. 3. On-site photos of the test site

The designed cross-sectional dimensions of the access tunnel are 8.0 × 8.3 m. Fig. 4 illustrates the blast network design for the pilot tunnel enlargement in the access tunnel. The blast hole diameter is 42 mm, with a drilling depth of 5.0 m and a single excavation advance of 4.5 - 5.0 m. The explosive used is No. 2 emulsion rock explosive with a diameter of 32 mm. To control blasting-induced vibrations, millisecond delay blasting technology is employed, with a delay time of 50 ms between adjacent segments. The blasting process is divided into seven segments (M1~M13).

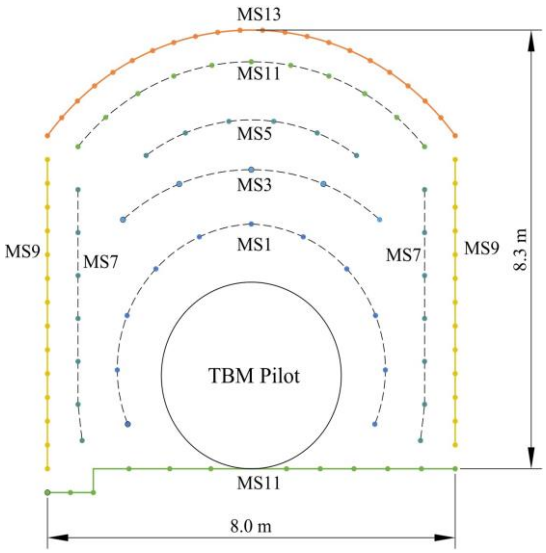

Fig. 4. Blasting network design diagram

2.2. Comparison of construction durations for different excavation methods

In the "Small-Diameter TBM Pilot Tunnel + Drill-and-Blast Enlargement" method, the free surface created by the pilot tunnel eliminates the need for cut blasting during the enlargement process, thereby providing the potential to increase the excavation advance rate. Theoretically, the excavation speed of drill-and-blast enlargement under free surface conditions can be significantly higher than that of the full-face drill-and-blast method. This necessitates the design of a rational advance rate for drill-and-blast enlargement based on site-specific conditions to fully leverage the construction schedule advantages of the combined TBM pilot tunnel and drill-and-blast method. To determine the optimal advance rate for drill-and-blast enlargement, this study begins with a theoretical analysis.

Assuming the total tunnel excavation length is L, the excavation speed of the full-face drill-and-blast method is V_f, the excavation speed of the drill-and-blast enlargement method is V_{pd}, and the excavation speed of the TBM (considering installation and maintenance) is V_{TBM}, the construction durations for the full-face drill-and-blast method and the TBM pilot tunnel with drill-and-blast enlargement method are as follows:

$$T_f = {}^{L}/_{V_f} \tag{1}$$

$$T_p = T_{pd} + T_{TBM} = {}^{L}/_{V_{pd}} + {}^{L}/_{V_{TBM}} \tag{2}$$

where, T_f represents the construction duration for the full-face drill-and-blast method; T_p denotes the construction duration for the TBM pilot tunnel combined with drill-and-blast enlargement; T_{pd} is the construction duration for the drill-and-blast enlargement; and T_{TBM} refers to the construction duration for the TBM pilot tunnel excavation.

The condition for the TBM pilot tunnel with drill-and-blast enlargement method to have a shorter construction duration than the full-section drill-and-blast method is $T_p<T_f$, which can be expressed as:

$$\frac{V_{pd} \cdot V_{TBM}}{V_{pd} + V_{TBM}} > V_f \tag{3}$$

In general, when the cross-sectional area of the designed tunnel excavation remains constant, the construction duration for the full-face drill-and-blast method can be estimated based on engineering experience. Assuming V_f is known, the relationship between V_{pd} and V_{TBM} can be expressed as:

$$V_{pd} > \frac{V_f \cdot V_{TBM}}{V_{TBM} - V_f} = \frac{V_f}{1-\zeta},\ \zeta \in (0,1] \tag{4}$$

where, $\zeta = {}^{V_f}/_{V_{TBM}}$

As shown in equation (4), the excavation advance rate of the drill-and-blast enlargement method depends on the ratio ζ between the excavation advance rates of the full-face drill-and-blast method and the TBM method. When ζ approaches 0, the required excavation advance rate for the drill-and-blast enlargement decreases; conversely, as it approaches 1, the required advance rate increases. If the excavation advance rate of the full-face drill-and-blast method is half that of the TBM method, the time-saving advantage of the TBM pilot tunnel with drill-and-blast enlargement method can only be realized when the advance rate of the drill-and-blast enlargement is at least twice that of the full-face drill-and-blast method.

Based on a one-month field study, the average excavation advance rate of the 2# construction branch tunnel was approximately 3–3.5 m per blast, while the average excavation advance rate of the test tunnel (access tunnel) was about 4.5–5.0 m per blast. Due to the operational constraints of the drill-and-blast method, such as post-blast ventilation and mucking, and considering the favorable rock mass integrity and stability revealed during excavation (classified as II-grade rock), the occurrence of re-drilling and re-blasting was minimal. Both tunnel sections achieved an actual blasting frequency of 2 blasts per day. Consequently, the daily excavation advance rate for the full-face drill-and-blast method was approximately 6–7 m/day, while the daily excavation advance rate for the drill-and-blast enlargement method reached 9–10 m/day.

Due to time constraints during on-site construction, the complete excavation duration of the TBM pilot tunnel could not be tracked, and its excavation advance data was not directly obtained. Therefore, the TBM excavation efficiency was estimated based on literature data. According to Farrokh [7], the excavation rate of a TBM is closely related to its diameter and the stress environment of the tunnel. Under the average stress level

of approximately 10 MPa in the access tunnel, the theoretical excavation speed of the TBM is estimated to be 2.2 m/h. However, factors such as equipment maintenance, support operations, crew shifts, and delays in muck transportation result in non-working time accounting for 70%–80% of the total construction period, leaving the actual TBM utilization rate at only 20%–30% [12]. Based on these considerations, the actual excavation speed of the TBM is calculated to be approximately 0.44–0.66 m/h, translating to a daily excavation advance rate of 10.56–15.84 m/day.

Under ideal construction conditions (i.e., an excavation advance rate of 7 m/day for the full-face drill-and-blast method and 15.84 m/day for the TBM pilot tunnel), calculations based on equation (4) indicate that the time-saving advantage of the TBM pilot tunnel + drill-and-blast enlargement method can only be realized if the excavation advance rate of the drill-and-blast enlargement method reaches approximately 12.5 m/day. If other conditions remain unchanged, to ensure the time efficiency of this method, the single-blast excavation advance rate for the enlargement process must reach 6 m or more. This indicates that, under the current excavation advance rate conditions, the time-saving advantage of the TBM pilot tunnel combined with the drill-and-blast enlargement method has not been effectively realized at the experimental site.

2.3. Field tests on rock damage from blasting enlargement

The previous analysis indicates that the current blasting excavation advance rate for TBM pilot tunnel + drill-and-blast enlargement does not meet the theoretical requirements, resulting in the method's time-saving advantage not being realized. To address this, increasing the excavation advance rate is necessary. However, increasing the advance rate may potentially expand the damage zone around the rock mass. Therefore, field tests on rock mass damage caused by TBM pilot tunnel + drill-and-blast enlargement are essential. A single-borehole acoustic monitoring test for blasting enlargement was conducted at the JC0+600 section. The layout of the acoustic boreholes is shown in Fig. 4, with a total of four symmetrically distributed test boreholes. The upper layer includes two boreholes (Borehole 1# and Borehole 3#), each with a depth of 15.5 m, while the lower layer includes two boreholes (Borehole 2# and Borehole 4#), each with a depth of 16.0 m. During the tests, the acoustic transducer was gradually moved from the bottom of each borehole toward the borehole opening, with measurements taken at intervals of 0.25 m. This ensured high-resolution monitoring of the damage characteristics around the boreholes.

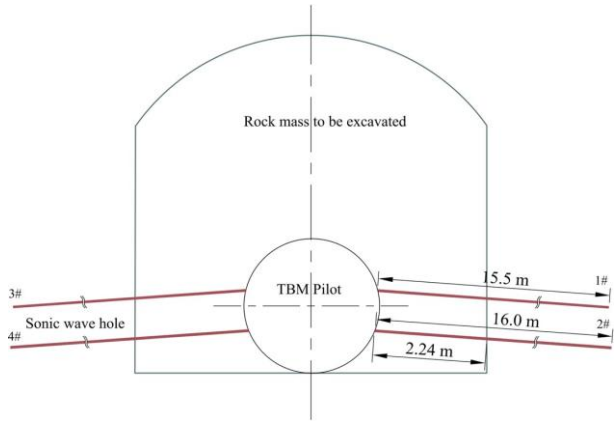

Fig. 5. Schematic diagram of acoustic borehole layout

Fig. 6. Field acoustic wave testing

The degree of volumetric damage D can be expressed in terms of the relationship between wave velocities before and after blasting [13]:

$$D = 1 - E/E_0 = 1 - C^2/C_0^2 \tag{5}$$

where, E_0 represents the initial elastic modulus of the rock mass before blasting; E represents the elastic modulus of the rock mass after blasting; C_0 and C denote the longitudinal wave velocities of the rock mass before and after blasting, respectively.

When acoustic testing is employed, the post-blast wave velocity C at the same location is lower than the pre-blast wave velocity C_0, and the rate of change η can be expressed as:

$$\eta = \left[1 - C/C_0\right] \times 100\% \tag{6}$$

Substituting equation (6) into equation (5), the relationship between the rock mass damage degree D and the wave velocity change rate η can be expressed as:

$$D = 1 - \left(1 - \eta\right)^2 \tag{7}$$

When using the acoustic testing method to assess blasting damage or the quality of rock mass excavation, the evaluation criteria should adhere to the following provisions: when $\eta \leq 10\%$, the rock mass is undamaged or exhibits negligible damage; when $10\% < \eta \leq 15\%$, the rock mass experiences minor damage; and when $\eta > 15\%$, the rock mass is considered damaged. If $\eta > 10\%$, the rock mass is determined to have sustained blasting- induced damage, corresponding to a rock mass damage threshold of $D_{cr} = 0.19$.

To more clearly reflect the impact of blasting enlargement on the surrounding rock, the wave velocity change rate η defined by equation (6) was used to evaluate the effect of blasting enlargement on the surrounding rock. The results are shown in Fig. 7. As the rock mass excavation thickness is approximately 2.24 m, by analyzing the wave velocity change rate before and after blasting enlargement, the damage depths of the surrounding rock were determined as follows: approximately 1.25 m at Borehole 1#, 1.5 m at Borehole 2#, and 1.0 m at Borehole 4#. The results for Borehole 3# were deemed unreliable due to borehole collapse.

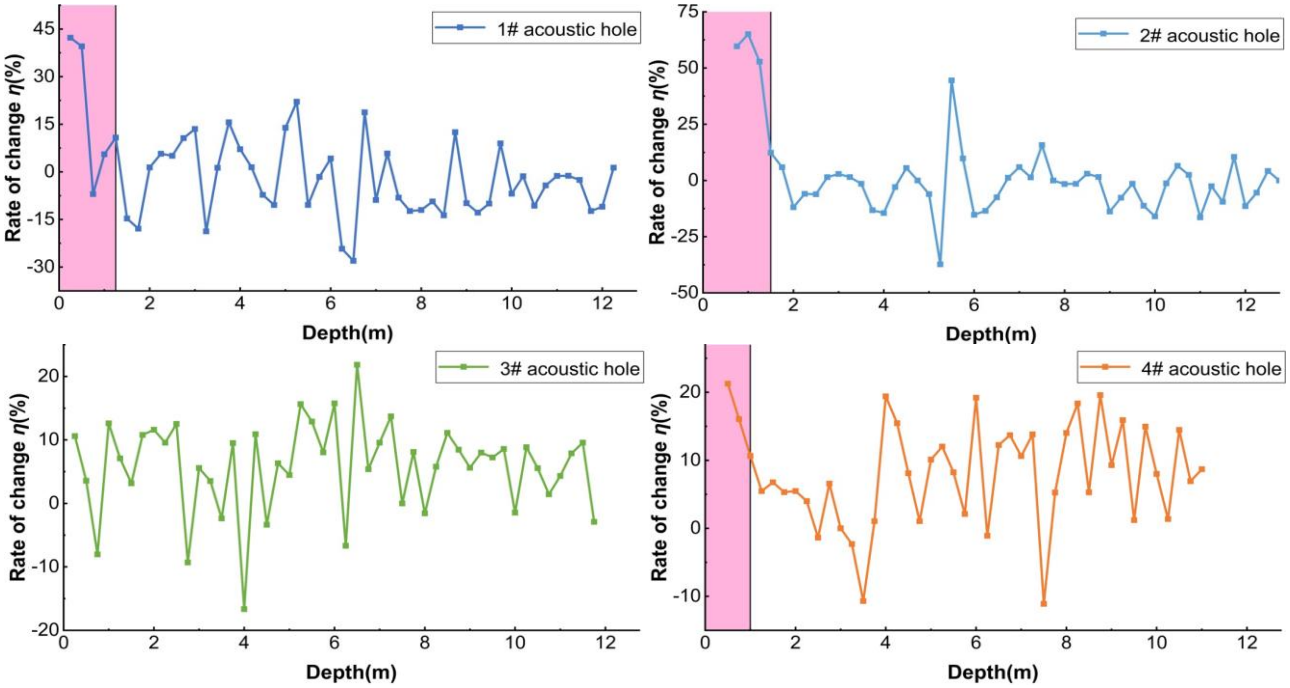

Fig. 7. Wave velocity change rates before and after blasting for each acoustic borehole

Based on the above analysis, the monitoring results of the rock mass damage range caused by TBM pilot tunnel and drill-and-blast enlargement are summarized in Table 2.

Table 2. Rock mass damage depths around each acoustic borehole during drill-and-blast enlargement

Monitoring Sites	Damage depth of surrounding rock (m)	Remark
1# acoustic hole	1.25	Borehole 3# experienced collapse, and its results are not considered reliable
2# acoustic hole	1.5	
3# acoustic hole	--	
4# acoustic hole	1.0	

3. Numerical simulation method and parameter calibration

Field monitoring experiments provided a direct understanding of the blasting damage effects during pilot tunnel expansion. However, due to limitations of field conditions, it is not possible to conduct experiments addressing the damage characteristics of surrounding rock under multiple factors. Additionally, field tests can only reflect the macroscopic effects of surrounding rock damage, making it difficult to capture the micro-crack propagation process and failure mechanisms during blasting expansion. Therefore, this study employs numerical simulation to conduct an in-depth investigation into the damage process of surrounding rock during drilling and blasting expansion under pilot tunnel conditions.

3.1. Numerical simulation method and parameter calibration

The UDEC-GBM method effectively models particle interactions, capturing essential rock mass properties such as Poisson's ratio, the tensile-to-compressive strength ratio, and interparticle interlocking [14, 15]. To calibrate the mesoscopic parameters, Si et al. identified a 3m × 6m model with a block size of 0.3m as the representative elementary volume (REV). Based on this, the block size in this study is adjusted to 0.5m, scaling the REV to 5m × 10m. To ensure quasi-static conditions, the loading rate is set at 0.05 m/s. The blocks follow elastic constitutive behavior, while contact interactions are governed by the Coulomb slip model.

Fig. 8 shows the stress-strain curve from uniaxial compression tests on the REV model. The calibrated elastic modulus and uniaxial compressive strength of the rock mass are 62.2 GPa and 250.5 MPa, respectively, with errors of 5.3% and 1.9%, both within acceptable limits. The mechanical parameters are summarized in Table 3, and the macroscopic properties of the model are listed in Table 4.

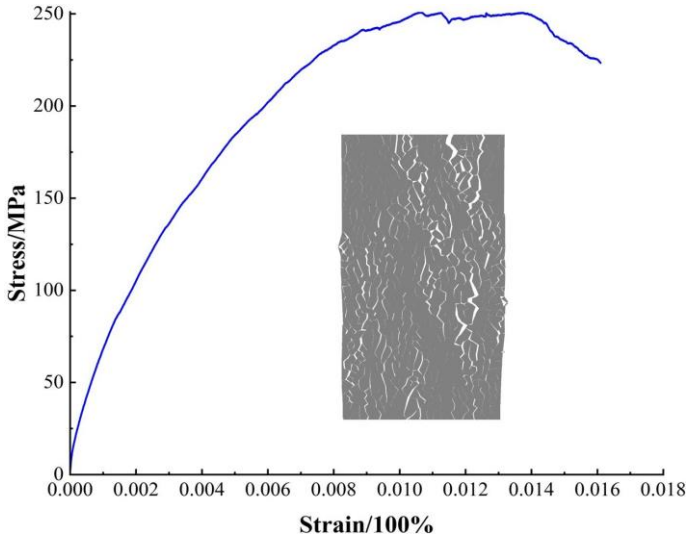

Fig. 8. Uniaxial Compression Stress-Strain Curve under REV Conditions

Table 3. Calibration results of micromechanical parameters for rock mass

Rock mass Properties	Target value	Calibrated	Error (%)	Contacts Properties	Calibrated
Young's modulus/GPa	65.7	62.2	5.3	Normal stiffness/GPa·m^{-1}	5500
UCS/MPa	245.9	250.5	1.9	Shear stiffness/GPa·m^{-1}	4000

Table 4. Macroscopic mechanical parameters of the model

Density (kg/m^3)	Compressive strength (MPa)	Tensile strength (MPa)	Elastic modulus *E* (GPa)	Poisson's Ratio *u*	Friction angle tgj	Cohesion (MPa)
2630	250.5	2.0	62.2	0.17	1.0	2.0

To perform numerical simulations of blasting damage, the blasting impact load model must first be determined based on the characteristics of the blasting load. For segmented charges or decoupled charge structures, the detonation pressure P_W is calculated using [16]:

$$P_W = \frac{\rho_e V_d^2}{2(\gamma+1)}\left(\frac{d_b}{d_e}\right)^{-2\gamma}\left(\frac{l_b}{l_e}\right)^{-\gamma} n \tag{8}$$

where, ρ_e is the explosive density, V_d is the detonation velocity, γ is the adiabatic exponent of the gaseous explosion products. Other parameters include the borehole diameter d_b, explosive charge diameter d_e, borehole charge segment length l_b, total explosive length l_e, and the amplification factor n [17].

According to blast cavity expansion theory, the peak pressure P_0 at the crushed zone boundary, representing the triangular blasting load's peak, is given by:

$$P_0 = P_W\left(\frac{1}{d}\right)^3 \tag{9}$$

where, d is the ratio of the crushed zone radius to the explosive charge radius, typically taken as 2 to 3.

The loading method adopts the equivalent load approach proposed by Lu et al. [18, 19]. In this method, the equivalent load is applied to the plane defined by the borehole centerline and axis, with its effective range corresponding to the length of the explosive charge segment. The magnitude of the equivalent load is calculated as:

$$P_e = \left(\frac{d_b}{a} \right) P_0 \tag{10}$$

where, a is the distance between adjacent borehole centerlines.

In this study, equivalent blasting loads are uniformly distributed as nodal pressures along the excavation contour, oriented perpendicular to the contour. Explosive and blasting parameters are listed in Table 5. The time-history curve of the triangular blasting load is illustrated in Fig. 9. The pressure rise time t_1 is set to 100μs, and the positive pressure duration t_2 is 600μs.

Table 5. Explosive and blasting parameters

Explosive density *ρe* (kg/m³)	**Detonation velocity *Vd* (m/s)**	**Borehole diameter *db* (mm)**	**Charge diameter *de* (mm)**
1150	4400	42	32
Segmented charge length *lb* (m)	**Charge length *le* (m)**	**Centerline distance *a* (m)**	**Equivalent load *Pe* (MPa)**
2.4	0.9	0.5	15.60

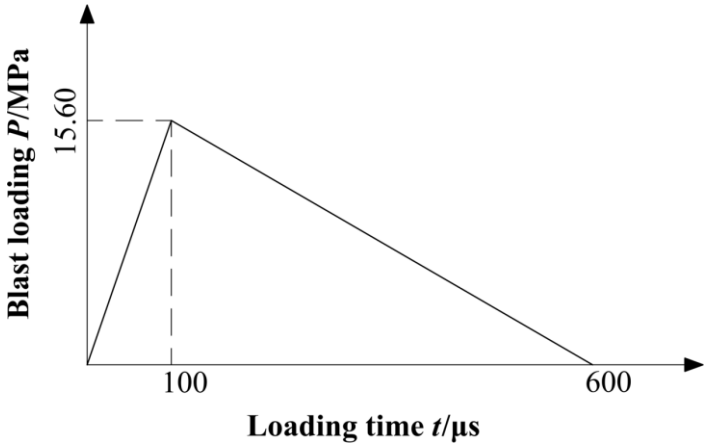

Fig. 9. Blasting load time-history curve

Rayleigh damping is utilized in this study's dynamic calculations [20]. In UDEC, its implementation requires defining the minimum central frequency f_{min} and the minimum critical damping ratio ξ_{min} [21]. The value of f_{min} is determined through undamped dynamic simulations, where the time-history velocity near the tunnel sidewall is analyzed, as shown in Fig. 10. A Fourier transform of this velocity yields the power spectrum as shown in Fig. 11, from which is identified as approximately 177 Hz. For rock materials, ξ_{min} typically ranges from 2% to 5%, with 5% selected in this study [22].

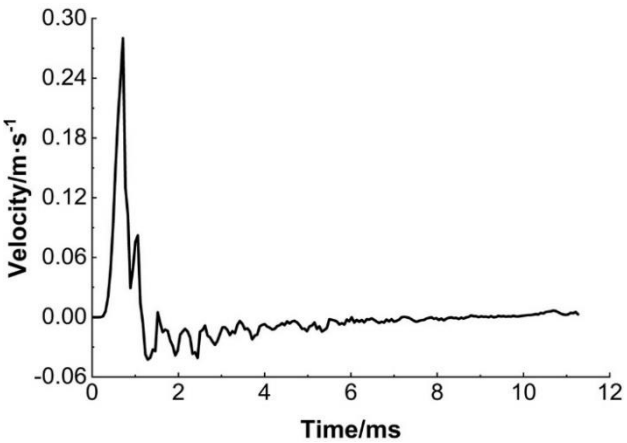

Fig. 10. Velocity time-history curve

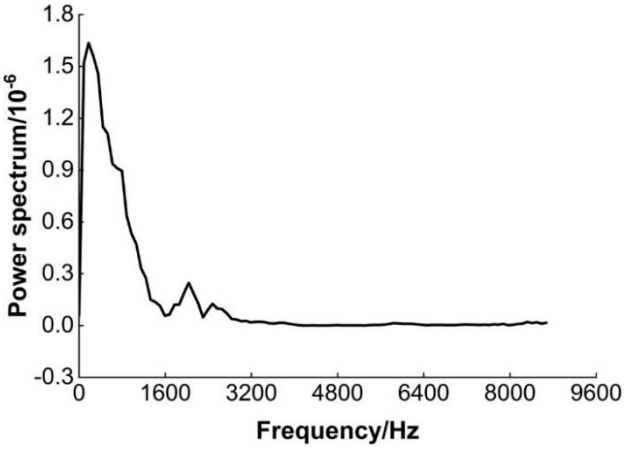

Fig. 11. Velocity time-history power spectrum

3.2. Validation of calculation results

Under the combined effects of excavation unloading and blasting impact, stress near the tunnel's free surface is released, generating tensile and shear stress zones. When these stresses exceed the surrounding rock's tensile and shear strength, significant micro-crack propagation occurs. Fig. 12 compares the numerical simulation results with field measurements of blasting damage, focusing on micro-crack propagation induced by excavation unloading and blasting loads. The simulated blasting damage depth is 1.75m, closely aligning with the field-measured depth of 1.5m obtained through single-borehole acoustic monitoring. This agreement demonstrates the feasibility of using micro-crack propagation as a method to characterize the damage zone depth.

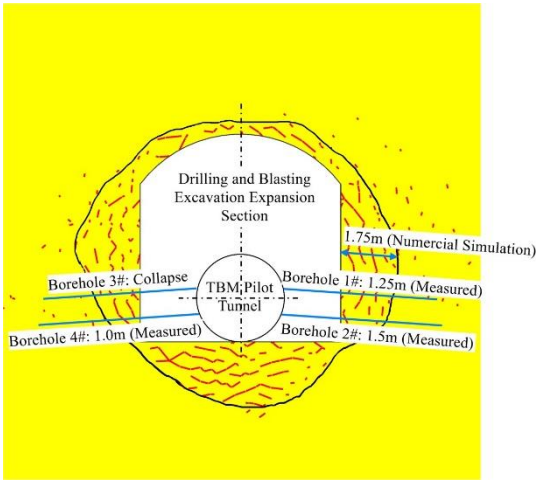

Fig. 12. Comparison of field measurements and numerical simulation results

The cumulative damage process of the model under blasting loads is represented by the ratio of the length of failed contacts to the total contact length within the model [23, 24]. Its specific definition is as follows:

$$D_c = \frac{L_t + L_s}{L_c}, \qquad D_t = \frac{L_t}{L_c}, \qquad D_s = \frac{L_s}{L_c} \tag{11}$$

where, D_c, D_t and D_s represent the total damage degree, tensile damage degree, and shear damage degree, respectively; L_c, L_t and L_s denote the total failed contact length, tensile failed contact length, and shear failed contact length, respectively.

By implementing the damage degree defined in equation (11) using a FISH function in UDEC, the corresponding program can be developed and invoked to obtain the variation curves of each damage degree over calculation time, as shown in Fig. 13. The results indicate that tensile failure (Ten-F), shear failure (She-F), and total damage (Tot-F) all increase with computation time. When the computation time reaches approximately 4ms, the damage degree ceases to change, indicating that the explosive stress wave no longer induces further damage to the surrounding rock. Throughout the process of explosive stress wave action, the proportion of shear failure is significantly higher than that of tensile failure. This observation aligns with the findings of Wang et al. [24] and Gao et al. [25].

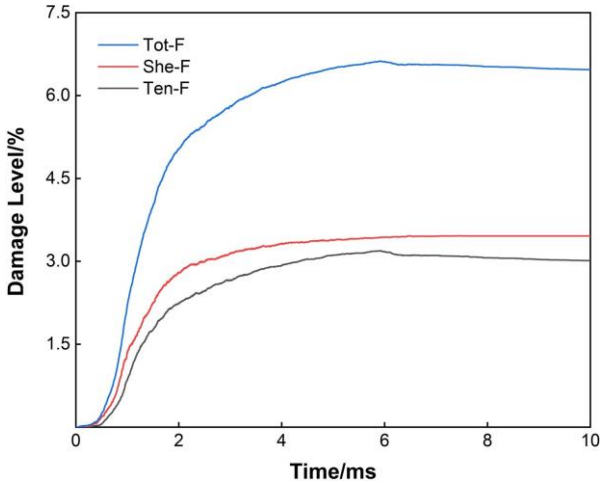

Fig. 13. The evolution process of damage level with mechanical time

4. Numerical simulation of rock mass damage effects

4.1. Influence of burial depth

The in-situ stress levels were set at 0.125*F*, 0.25*F*, 0.5*F*, *F*, 2*F* and 3*F*, where *F* represents the vertical stress at a burial depth of 450 m, with a lateral pressure coefficient of 1.6. The distribution of micro-cracks in the surrounding rock during tunnel excavation and the induced macroscopic failure were analyzed, as shown in Fig. 14. The calculation results indicate that with increasing burial depth, the number of cracks in the surrounding rock increases significantly, the affected range expands, and the damage depth deepens progressively. After blasting enlargement, the cracks around the tunnel are predominantly shear cracks. Under the combined effects of excavation unloading and blasting loads, micro-cracks mainly distribute and propagate along the direction of the maximum principal stress.

As the in-situ stress level increases, micro-cracks gradually extend and coalesce, with the proportion of tensile cracks increasing significantly. Compared to shear failure, the lower tensile strength of the rock leads to weaker resistance against tensile stress, making tensile cracks the primary factor controlling the macroscopic failure of the surrounding rock. During the blasting enlargement process, the combined effects of unloading and impact loads cause tensile micro-cracks near the tunnel to expand and coalesce, forming macroscopic tensile cracks. These cracks further extend and coalesce, eventually evolving into tensile failure. The comparative analysis of micro-crack distribution shows that the macroscopic failure of the surrounding rock coincides with the distribution area of interconnected tensile cracks. Tensile failure predominantly occurs at burial depths of 900 m and 1350 m, while no macroscopic tensile failure is observed at shallow depths.

These findings demonstrate that in-situ stress levels significantly enhance the tensile failure effects of drill-and-blast enlargement on the surrounding rock. With increasing in-situ stress levels, the tensile failure on both sides of the tunnel walls becomes more pronounced, requiring careful consideration in construction design.

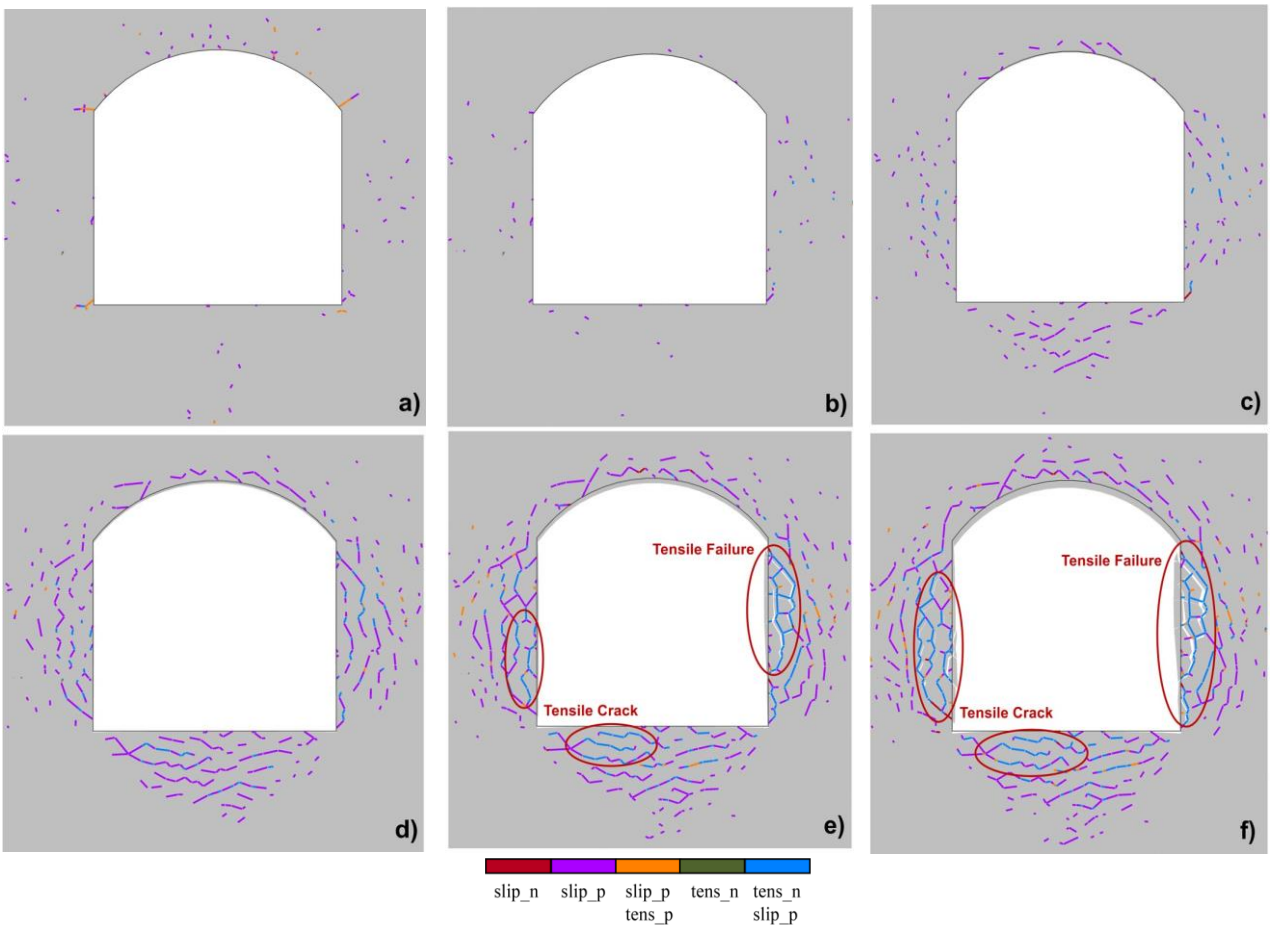

Fig. 14. Conditions calculation results of blast-induced crack damage zones under different in-situ stress levels (*burial depths*) *with pilot tunnel conditions: a*) *Burial depth = 56.25 m, b*) *Burial depth = 112.5 m, c*) *Burial depth = 225 m, d*) *Burial depth = 450 m, e*) *Burial depth = 900 m, f*) *Burial depth = 1350 m*

Fig. 15 presents the statistical results of damage forms under various in-situ stress conditions. It can be observed that with increasing in-situ stress levels, the total damage degree, shear damage degree, and tensile damage degree all increase to varying extents. However, the rate of increase in damage levels gradually diminishes as the in-situ stress levels continue to rise. Additionally, the proportion of tensile damage steadily increases, which is consistent with the results of the micro-crack distribution analysis.

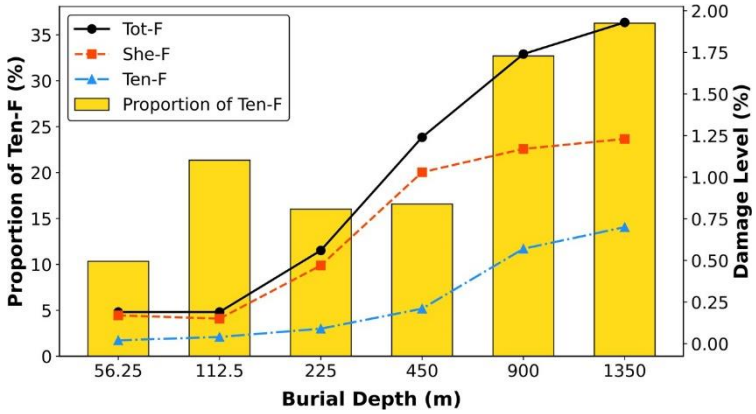

Fig. 15. Statistical analysis of damage degree under different in-situ stress levels (*burial depths*)

Fig. 16 shows the calculation results of the blasting-induced crack damage zone under full-face drill- and-blast excavation conditions. It can be observed that the microcrack propagation patterns around the tunnel under full-face drill-and-blast excavation are similar to those under TBM pilot tunneling and subsequent enlargement, despite differences in in-situ stress levels. With increasing burial depth, rock mass damage is characterized by an expansion of the crack range, an increase in crack density, and a significant rise in the proportion of tensile cracks.

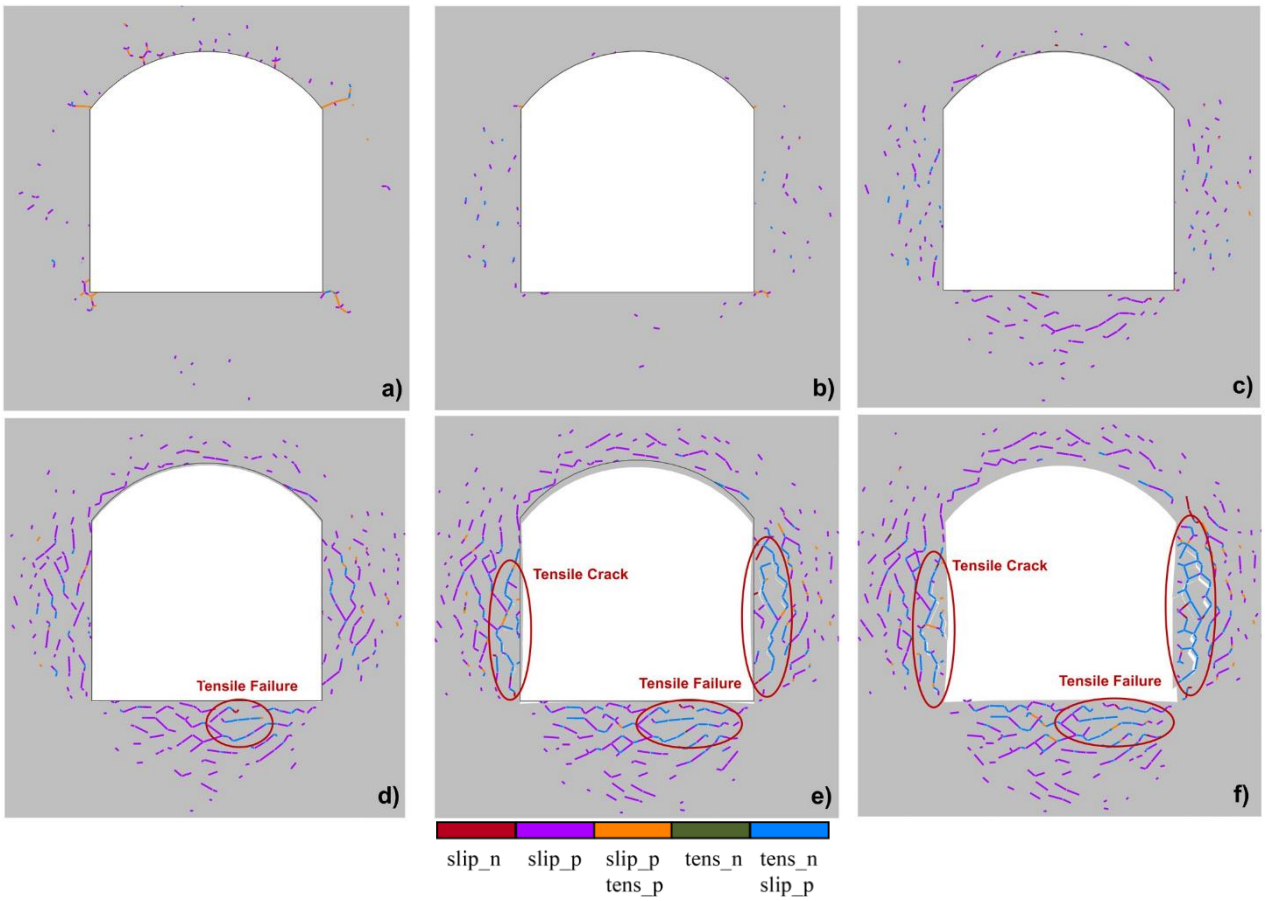

Fig. 16. Calculation results of blast-induced crack damage zones under full-face drilling and blasting expansion at different in-situ stress levels (*burial depths*)*: a) Burial depth = 56.25m b) Burial depth = 112.5m c) Burial depth = 225m, d) Burial depth = 450m, e) Burial depth = 900m, f) Burial depth = 1350m*

From the perspective of macroscopic failure, the full-face drill-and-blast method exhibits minor macroscopic cracks induced by interconnected tensile cracks in the lower right portion of the tunnel floor at a burial depth of 450m. This indicates that, compared to the TBM pilot tunnel with drill-and-blast enlargement, the transient unloading effect of the full-section drill-and-blast method is more intense.

Fig. 17 presents the statistical results of damage degrees. It shows that at shallow burial depths (450m and below), the surrounding rock damage is predominantly governed by shear cracks. As the burial depth increases, particularly beyond 450m, the proportion of tensile cracks increases significantly. However, shear cracks remain the primary factor in controlling rock mass damage.

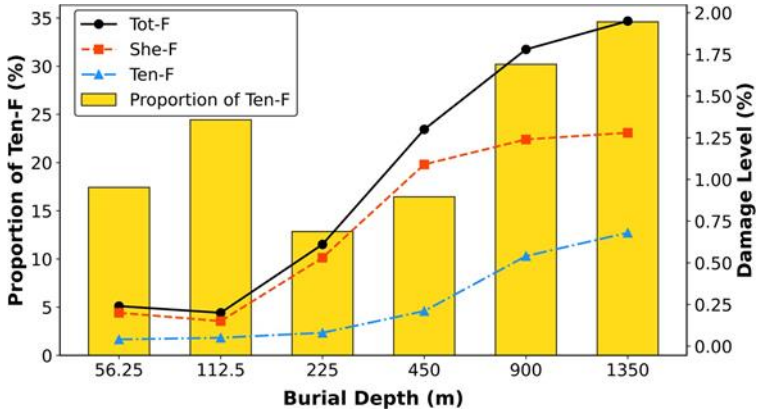

Fig. 17 Statistical analysis of damage degree under different in-situ stress levels (*burial depths*)

Fig. 18 illustrates the relationship between burial depth and surrounding rock damage degree for full-face blasting excavation and the TBM pilot tunnel method. With burial depth increasing from 56.25m to 1350m, the damage degree rises significantly, highlighting burial depth as a key factor in rock damage during blasting excavation. Under shallow burial conditions (burial depth < 450m), the damage degree for full-face blasting is higher than for the TBM pilot tunnel method, demonstrating the latter's better control of surrounding rock damage. However, as burial depth increases, this advantage diminishes, with only a 1% improvement at 1350m. The results emphasize the effectiveness of the TBM pilot tunnel method in mitigating rock damage at shallow burial depths, though its advantages decrease with increasing depth.

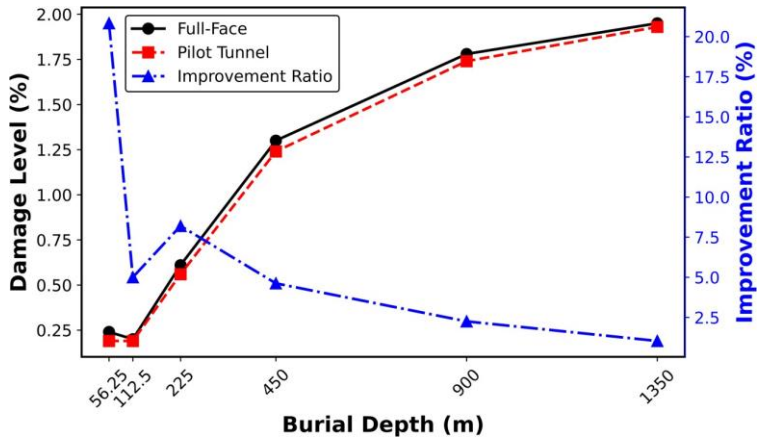

Fig. 18. Comparison of damage degree

4.2. Influence of lateral pressure coefficient

Fig. 19 illustrates the crack distribution and failure characteristics of the surrounding rock during TBM pilot tunnel drill-and-blast expansion under different lateral pressure coefficients. As the lateral pressure coefficient increases from 0.5 to 2.5, significant changes occur in the crack distribution and failure modes of the surrounding rock. Under low lateral pressure coefficient conditions (0.5 to 1.0), micro-cracks around the tunnel are predominantly shear cracks, with fewer tensile cracks. In contrast, under high lateral pressure coefficients (1.6 to 2.5), the tensile stress on both sides of the sidewalls increases significantly, leading to a substantial increase in the number of tensile cracks, which gradually connect to form through-going tensile failure zones. Simultaneously, tensile cracks at the tunnel crown and invert also become more pronounced.

Notably, when the lateral pressure coefficient reaches 2.0 and 2.5, the through-going tensile cracks near the sidewalls and tunnel invert induce large-scale macroscopic tensile failure. Regarding crack distribution, at a lateral pressure coefficient of 0.5, the cracks are more dispersed and primarily concentrated on the left and right sides, consistent with results reported in the literature [26]. As the lateral pressure coefficient increases, the cracks progressively cluster and extend deeper into the surrounding rock, a phenomenon particularly evident in the tunnel floor region. This indicates that as the lateral pressure coefficient increases, the damage mechanism of the surrounding rock transitions from shear failure to tensile failure, with a tendency to extend deeper into the rock mass. Additionally, under high lateral pressure coefficients, tensile failure in the sidewall regions becomes particularly prominent

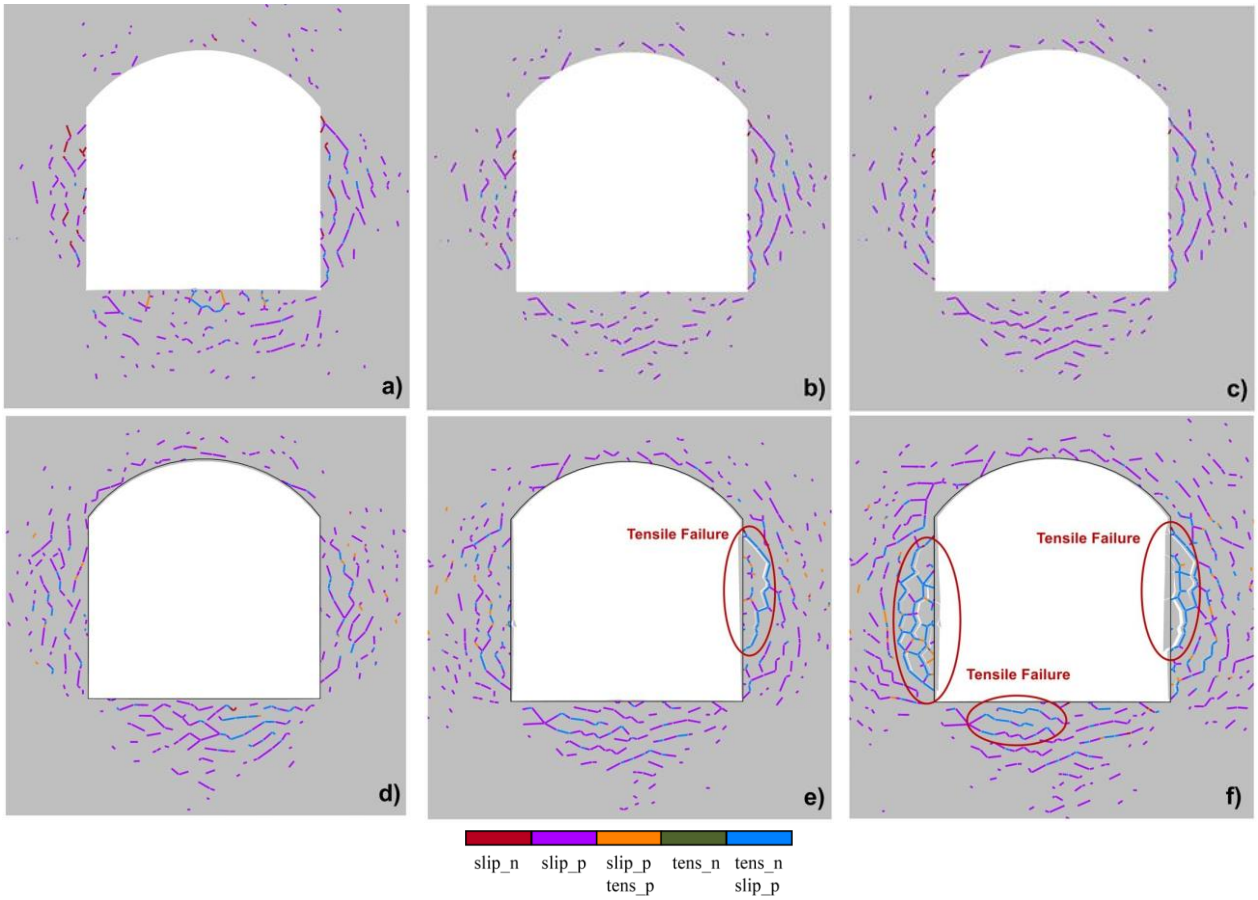

Fig. 19. Conditions calculation results of blast-induced crack damage zones under different lateral pressure coefficients: with pilot tunnel conditions. a) Lateral Pressure Coefficient = 0.5; b) Lateral Pressure Coefficient = 0.75; c) Lateral Pressure Coefficient = 1.0; d) Lateral Pressure Coefficient = 1.6; e) Lateral Pressure Coefficient = 2.0; f) Lateral Pressure Coefficient = 2.5

Fig. 20 presents the statistical results of surrounding rock damage under different lateral pressure coefficients. As shown in the figure, with the lateral pressure coefficient increasing from 0.5 to 2.5, the total damage (Tot-F), shear damage (She-F), and tensile damage (Ten-F) exhibit a trend of initially decreasing gradually and then rising rapidly. The surrounding rock damage reaches its minimum value when the lateral pressure coefficient is around 0.75. However, when the lateral pressure coefficient exceeds 1, especially beyond 2, the damage level increases significantly. At lower lateral pressure coefficients (0.5 to 1.0), the damage to the surrounding rock is predominantly shear damage, with a relatively small proportion of tensile damage. As the lateral pressure coefficient increases further (1.6 to 2.5), the proportion of tensile damage rises markedly, indicating a transition in the failure mode of the surrounding rock from shear-dominated to a tensile-shear composite failure. Notably, at a lateral pressure coefficient of 2.5, the proportion of tensile damage reaches approximately 30%, with tensile damage effects becoming more prominent in sidewalls and other critical areas. Moreover, the trend of total damage growth aligns with the changes in both shear and tensile damage, highlighting the significant impact of increasing lateral pressure coefficients on the overall damage to the surrounding rock [27].

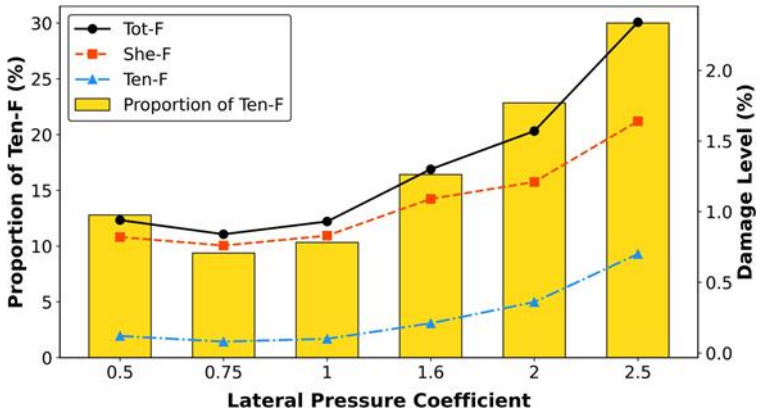

Fig. 20. Statistical analysis of damage degree under different lateral pressure coefficient

4.3. Discussion of results

The direction of the principal stress plays a dominant role in the initial spatial distribution of damage during blasting excavation. The stress release and redistribution caused by excavation unloading lead to instantaneous stress changes around the tunnel. The rapid release of radial stress results in the formation of tensile stress zones near the tunnel boundary, accompanied by the emergence of a small number of tensile cracks, which are primarily distributed along the direction of the principal stress. As the in-situ stress level increases, tensile cracks near the sidewalls of the tunnel gradually extend and coalesce, forming macroscopic tensile failure. This indicates that the structural stress, represented by the lateral pressure coefficient, and the in-situ stress significantly influence tensile failure in the surrounding rock during blasting expansion.

Following blasting expansion, the number of shear cracks is substantially greater than that of tensile cracks. Shear cracks are distributed more deeply near the left and right sidewalls and the floor of the tunnel, while their distribution depth near the crown is relatively shallow. Given that the tensile strength of rock is far lower than its compressive strength, the macroscopic failure of the rock mass is predominantly governed by tensile failure driven by tensile cracks. With increasing burial depth, the proportion of tensile cracks gradually rises, becoming the dominant factor in the failure of the surrounding rock. This explains why the surrounding rock is more prone to damage and failure under deep burial conditions.

The lateral pressure coefficient significantly affects the crack distribution characteristics around the tunnel by altering the principal stress distribution in the surrounding rock. When the lateral pressure coefficient is less than 1, the maximum principal stress direction of the surrounding rock aligns with the vertical gravitational direction before excavation. During drill-and-blast expansion, as the supporting effect of the surrounding rock is removed, the stress distribution adjusts rapidly, leading to extensive tensile failure in the crown and invert regions. Conversely, when the lateral pressure coefficient exceeds 1, the initial stress field of the surrounding rock is dominated by horizontal stress. Under the same burial depth, the influence of horizontal stress becomes more pronounced, resulting in distinct crack distribution patterns. From a mechanistic perspective, when the lateral pressure coefficient is low, vertical stress dominates, and the rapid unloading of vertical stress during excavation makes the crown and invert more susceptible to tensile failure. However, as the lateral pressure coefficient increases, the influence of horizontal stress strengthens, reducing the tensile failure effects in the crown and invert while generating significant tensile stress concentration in the sidewalls. This stress redistribution induces a shift in the failure mode, with the failure of the crown and invert transitioning from tensile failure to compressive-shear failure, while tensile damage in the sidewalls intensifies and eventually evolves into the dominant failure mode. The lateral pressure coefficient has a significant impact on the failure mode of surrounding rock, with tensile failure in the sidewalls becoming particularly prominent under high lateral pressure coefficient conditions.

5. Sensitivity analysis

The burial depth of the tunnel and the lateral pressure coefficient are critical factors affecting the degree of damage to the surrounding rock during blasting-induced expansion. Variations in burial depth modify the in-situ stress field acting on the surrounding rock, influencing the magnitude and distribution of stress concentration zones. These changes play a key role in determining the fracture mechanisms and pathways of damage evolution in the rock mass [28]. Similarly, the lateral pressure coefficient influences the stress distribution around the tunnel, thereby affecting the distribution pattern and propagation paths of micro-cracks in the surrounding rock during blasting expansion. This adjustment impacts the redistribution of stress

and the resulting concentration effects, which in turn govern the fracture behavior and damage progression of the surrounding rock. By performing a sensitivity analysis on different burial depths and lateral pressure coefficient, a quantitative understanding of the primary factors influencing rock damage can be achieved, offering insights into the underlying mechanisms and patterns of their effects [29, 30].

The relationship between tunnel burial depth, lateral pressure coefficient, and surrounding rock damage degree was fitted to corresponding functions. The fitting results are presented in Fig. 21. As shown in Fig. 21 a), the relationship between tunnel burial depth and surrounding rock damage degree can be described by equation (12), with a fitting coefficient of determination R^2 of 0.9480, indicating a strong fit. Fig. 21 b) illustrates the relationship between lateral pressure coefficient and surrounding rock damage degree. The relationship follows a quadratic function described by equation (13), with an R^2 value of 0.9933, demonstrating a good fitting performance.

$$D = 0.0177 \times D_e^{0.6613} \tag{12}$$

$$D = 0.4572 \times L_p^2 - 0.666 \times L_p + 1.1326 \tag{13}$$

where, D is the degree of surrounding rock damage, D_e is the tunnel burial depth, L_p is the lateral pressure coefficient.

The fitting results indicate that the relationship between tunnel burial depth *De* and the degree of surrounding rock damage *D* follows a power function growth pattern. As the burial depth increases, the degree of surrounding rock damage increases rapidly, demonstrating high sensitivity to burial depth. In contrast, the relationship between the lateral pressure coefficient and the surrounding rock damage exhibits a distinct quasi-symmetric pattern. As the lateral pressure coefficient increases, the damage level of the surrounding rock decreases initially and then increases. Based on the fitting results, influenced by the shape of the excavated tunnel, the minimum damage level occurs at a lateral pressure coefficient of approximately 0.73.

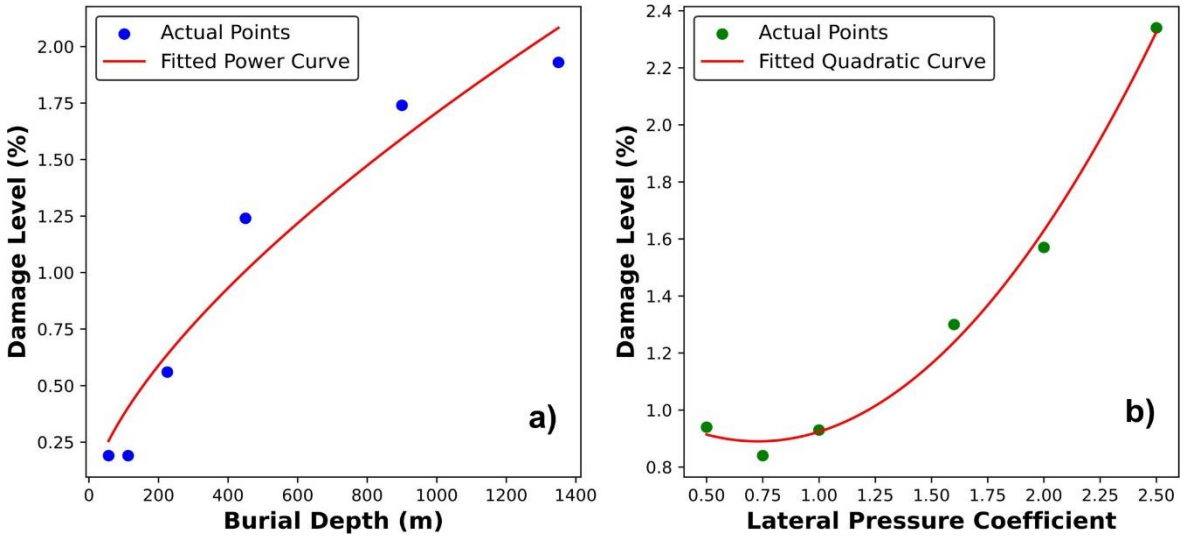

Fig. 21. Fitting results for damage degree: a) Relationship between tunnel burial depth and damage level, b) Relationship between lateral pressure coefficient and damage level

The nonlinear growth trend observed in the relationship between burial depth, lateral pressure coefficient, and surrounding rock damage indicates that the degree of rock damage increases significantly with the rise in both burial depth and lateral pressure coefficient. To further validate the contribution of these two influencing factors to the degree of surrounding rock damage, a significance test is conducted to confirm the statistical significance of their impacts.

To establish a multivariate nonlinear regression model between burial depth (D_e), lateral pressure coefficient (L_p), and the surrounding rock damage degree (D), the general expression can be formulated as follows:

$$D = b_1 \cdot D_e^{a_1} + b_2 \cdot L_p^2 + b_3 \cdot L_p + \varepsilon \tag{14}$$

where, b_1, b_2 and b represent the regression coefficients of the respective variables, a_1 is the exponent of the power function, and ε is the error term.

By substituting the original data into the above equation, the multivariate nonlinear regression equation describing the relationship between burial depth, lateral pressure coefficient, and surrounding rock damage degree can be obtained:

$$D = 0.9026 D_e^{0.2095} + 0.0654 L_p^2 - 0.2758 L_p - 1.7843 \quad (15)$$

The R^2 value of 0.9619 for the above equation indicates that the model explains approximately 96.19% of the variation in the damage depth, demonstrating a reliable model fit. To quantify the relative contribution of the two factors to the surrounding rock damage degree, sensitivity analysis can be performed using equation (16). This analysis determines the normalized contribution rates, which quantify the relative influence of tunnel burial depth and pilot tunnel diameter on the degree of surrounding rock damage. The closer the normalized contribution rate of a variable is to 1, the greater its contribution to the damage degree of surrounding rock during drill-and-blast expansion.

$$C_I = \frac{b_i \cdot \left(X_i^{max} - X_i^{min} \right)}{\sum \left| b_i \right| \cdot \left(X_i^{max} - X_i^{min} \right)} \quad (16)$$

where, b_i represents the regression coefficient, while X_i^{max} and X_i^{min} denote the maximum and minimum values of the variable X_i, respectively.

The calculation results indicate that the relative contribution of tunnel burial depth to the degree of surrounding rock damage is 61.2%, while the lateral pressure coefficient contributes 38.8%. This demonstrates that, compared to the lateral pressure coefficient, tunnel burial depth has a greater influence on surrounding rock damage, serving as the primary factor. However, the lateral pressure coefficient also accounts for a significant relative contribution of 38.8%, approaching 40%. This underscores the importance of considering tectonic stress, represented by the lateral pressure coefficient, as a critical factor in the design of tunnel excavation in engineering projects.

6. Conclusions

This study employs the UDEC distinct element method, combined with field-measured data, to analyze the damage characteristics of the surrounding rock during the drill-and-blast expansion process of TBM pilot tunnels. The damage depth of the surrounding rock was measured using the single-hole ultrasonic method, and preliminary conditions for excavation advancement, highlighting the construction time advantage of the "Small-Diameter TBM Pilot Tunnel + Drill-and-Blast Expansion" method, were proposed. The effects of different stress levels and pilot tunnel sizes on the morphology and distribution of micro-cracks in the surrounding rock were examined. Finally, the relative contributions of tunnel burial depth and lateral pressure coefficient to the damage of surrounding rock during drill-and-blast expansion were investigated. The main conclusions are presented as follows:

(1) The full-face drill-and-blast method is limited by the effects of cut blasting and single-free-face confinement, resulting in an excavation advancement of typically 3–3.5m. In contrast, the "Small-Diameter TBM Pilot Tunnel + Drill-and-Blast Expansion" method effectively increases free faces for blasting through the pre-excavation of the TBM pilot tunnel, reducing the adverse impact of confinement and providing favorable conditions for improving excavation advancement. However, the pre-excavation process increases construction complexity, which may have a negative impact on the project schedule. The excavation advancement of the drill-and-blast expansion is significantly influenced by the ratio of excavation advancements between the full-face drill-and-blast method and the TBM method. A lower ratio results in reduced excavation advancement requirements, while a ratio approaching 1 leads to a substantial increase in excavation advancement. When the excavation advancements of the TBM and drill-and-blast expansion methods are equal and both are double that of the full-face drill-and-blast method, the time-saving advantage of the "Small-Diameter TBM Pilot Tunnel + Drill-and-Blast Expansion" method is fully realized, with lower construction requirements.

(2) The degree of surrounding rock damage demonstrates a positive power-law correlation with tunnel burial depth. As burial depth increases, the damage depth and crack density of the surrounding rock during drill-and-blast expansion rise significantly. Under varying burial depths, shear cracks dominate the damage mechanism within a certain range from the excavation surface, influenced by stress field adjustments induced by pilot tunnel excavation and subsequent expansion. However, increased burial depth intensifies transient unloading effects and secondary stress adjustments during blasting, leading to a significant increase

in the proportion of tensile cracks. This effect becomes particularly pronounced under deep burial conditions exceeding 450m, where tensile cracks rapidly penetrate and form failure zones near the sidewalls and invert, with tensile failure effects being most prominent at depths of 900m and 1350m. Moreover, the "Small-Diameter TBM Pilot Tunnel + Drill-and-Blast Expansion" method reduces surrounding rock damage by approximately 10% under shallow burial conditions compared to the full-face drill-and-blast method. However, this mitigation effect weakens with increasing burial depth.

(3) The influence of the lateral pressure coefficient on surrounding rock damage exhibits a trend of initially decreasing and then increasing. When the lateral pressure coefficient is less than 1, the maximum principal stress direction aligns with the gravitational direction, making the crown and invert more susceptible to tensile failure during drill-and-blast expansion. As the lateral pressure coefficient increases, the influence of horizontal stress becomes more pronounced, reducing tensile failure effects at the crown and invert while inducing significant tensile stress concentration in the sidewall regions. This results in the formation of through-going tensile cracks in the sidewalls and portions of the invert, eventually evolving into macroscopic tensile failure. Under high lateral pressure coefficient conditions, tensile failure effects in the sidewalls become particularly prominent.

Regression analysis and normalized contribution rate calculations indicate that the relative contribution of tunnel burial depth to surrounding rock damage is 61.2%, which is higher than the contribution of the lateral pressure coefficient at 38.8%. This suggests that surrounding rock damage is more sensitive to tunnel burial depth. However, it is noteworthy that under high lateral pressure coefficient conditions ($L_p \geq 2$), significant tensile failure zones still occur on both sides of the sidewalls even at a burial depth of 450m (moderate depth). This highlights that the influence of the lateral pressure coefficient on surrounding rock damage cannot be overlooked, even in shallow tunnels ($De < 450m$).

This study provides a preliminary analysis of the impact of the stress environment during tunnel excavation on surrounding rock damage and proposes initial excavation advancement conditions to leverage the time-saving advantages of the "Small-Diameter TBM Pilot Tunnel + Drill-and-Blast Expansion" method. However, it is important to note that the excavation cost of TBM is significantly higher than that of the drill-and-blast method, and this cost increases substantially with the diameter of the TBM pilot tunnel. This presents a challenge for the broader application of the "Small-Diameter TBM Pilot Tunnel + Drill-and-Blast Expansion" method. Additionally, the secondary stress field induced by the pilot tunnel size effect results in a stress environment during drill-and-blast expansion that differs significantly from that of the full-face drill-and-blast method. Future research will focus on addressing these issues in greater depth.

Acknowledgements

The authors gratefully appreciate the supports from the National Natural Science Foundation of China (No. 52379108). The first author of this paper is grateful to the Chinese Scholarship Council (Project number: 202406270103) for providing an opportunity to conduct the research described in this paper as a Visiting Research Student at University of Bologna.

References

[1] **Ji F., Lu J., Shi Y., et al.,** 2013
Mechanical response of surrounding rock of tunnels constructed with the TBM and drill-blasting method, Nat Hazards. https://doi.org/10.1007/s11069-012-0500-2

[2] **Bieniawski Z., Celada B., Galera J.**, et al., 2008
New applications of the excavability index for selection of TBM types and predicting their performance, ITA World Tunneling Congress

[3] **Man K., Liu X., Song Z.**, 2021
A new excavation technology of blasting combined with TBM, Geomatics, Natural Hazards and Risk 12. https://doi.org/10.1080/19475705.2021.1998231

[4] **Liu Q., Huang X., Gong Q.**, et al., 2016
Application and development of hard rock TBM and its prospect in China, Tunneling and Underground Space Technology. https://doi.org/10.1016/j.tust.2016.01.034

[5] **Janbaz S.**, 2017
Development of a production estimation model for tunnel boring machines (*TBMs*), University of Texas at Arlington

[6] **Serajiantehrani R., Janbaz S., Najafi M.**, et al., 2019
Impact of Tunnel Boring Machine Advance Rate for Pipeline Construction Projects, American Society of Civil Engineers. https://doi.org/10.1061/9780784482490.070

[7] **Farrokh E.**, 2013
Study of utilization factor and advance rate of hard rock TBMs, The Pennsylvania State University

[8] **Kong S., Choi S., Shim S.**, et al., 2021
Stability evaluation of TBM pilot tunnels to rear blasting using the protection shield, Applied Sciences. https://doi.org/10.3390/app11041759

[9] **Fan C., Qin J.**, Wang G., 2024
Construction mechanical characteristics of TBM pilot and enlargement method for ventilation tunnel of Wuhai pumped storage power station, Applied Sciences. https://doi.org/10.3390/app14051829

[10] **Pelizza S.**, 1991
Pilot bore excavation with TBM for the design and construction of larger tunnels, Tunneling and Underground Space Technology. https://doi.org/10.1016/0886-7798(91)90065-C

[11] **Miura K., Yagi H., Shiroma H.**, et al., 2003
Study on design and construction method for the New Tomei–Meishin expressway tunnels, Tunneling and Underground Space Technology. https://doi.org/10.1016/S0886-7798(03)00036-1

[12] **Rostami J.**, 2016
Performance prediction of hard rock Tunnel Boring Machines (*TBMs*) *in difficult ground*, Tunneling and Underground Space Technology. https://doi.org/10.1016/j.tust.2016.01.009

[13] **Ling T., Li S., Liu D.**, et al., 2023
Blasting Damage of Tunnel Rock Mass Based on Cumulative Effect, Rock Mech. Rock Eng. https://doi.org/10.1007/s00603-022-03128-8

[14] **Pan C., Li X., Zhao G.**, et al., 2025
Effect of meso-structure on quasi-static and dynamic tensile strength of rock: insights from a breakable grain-based model, Geomech. Geophys. Geo-Energ. Geo-Resour. https://doi.org/10.1007/s40948-024-00916-0

[15] **Wang X., Cai M.**, 2018
Modeling of brittle rock failure considering inter- and intra-grain contact failures, Computers and Geotechnics. https://doi.org/10.1016/j.compgeo.2018.04.016

[16] **Lu Y., Jin C., Wang Q.**, et al., 2023
Modeling Study on Cumulative Damage Effects and Safety Control Criterion of Open-Pit Final Slope Under Blasting, Rock Mech. Rock Eng. https://doi.org/10.1007/s00603-023-03656-x

[17] **Yang J., Lu W., Hu Y.**, et al., 2015
Numerical Simulation of Rock Mass Damage Evolution During Deep-Buried Tunnel Excavation by Drill and Blast, Rock Mech. Rock Eng. https://doi.org/10.1007/s00603-014-0663-0

[18] **Lu W., Yang J., Chen M.**, et al., 2011
An equivalent method for blasting vibration simulation, Simulation Modelling Practice and Theory, https://doi.org/10.1016/j.simpat.2011.05.012

[19] **Lu W., Yang J., Yan P.**, et al., 2012
Dynamic response of rock mass induced by the transient release of in-situ stress, International Journal of Rock Mechanics and Mining Sciences. https://doi.org/10.1016/j.ijrmms.2012.05.001

[20] **Spears R., Jensen S.**, 2012
Approach for Selection of Rayleigh Damping Parameters Used for Time History Analysis, Journal of Pressure Vessel Technology. https://doi.org/10.1115/1.4006855

[21] **Cruz C., Miranda E.**, 2017
A critical review of the rayleigh damping model, 16th World Conference on Earthquake, 16WCEE 2017

[22] **Naeim F., Kircher C.**, 2001
On the damping adjustment factors for earthquake response spectra, Struct. Design Tall Build. https://doi.org/10.1002/tal.180

[23] **Si Y., Liu J., Li F.**, et al., 2023
Roadways fracture response under varying dominant blasting frequencies and lateral pressure coefficients, International Journal of Impact Engineering. https://doi.org/10.1016/j.ijimpeng.2023.104761

[24] **Wang J., Apel D., Dyczko A.**, et al., 2022
Analysis of the damage mechanism of strainbursts by a global-local modeling approach, Journal of Rock Mechanics and Geotechnical Engineering. https://doi.org/10.1016/j.jrmge.2022.01.009

[25] **Gao Q., Stead D.**, 2014
The application of a modified Voronoi logic to brittle fracture modelling at the laboratory and field scale, International Journal of Rock Mechanics and Mining Sciences. https://doi.org/10.1016/j.ijrmms.2014.02.003

[26] **Zhu W., Liu J., Tang C.**, et al., 2005
Simulation of progressive fracturing processes around underground excavations under biaxial compression, Tunnelling and Underground Space Technology. https://doi.org/10.1016/j.tust.2004.08.008

[27] **Long Y., Liu J., Lei G.**, et al., 2020
Progressive fracture processes around tunnel triggered by blast disturbances under biaxial compression with different lateral pressure coefficients, Transactions of Nonferrous Metals Society of China. https://doi.org/10.1016/S1003-6326(20)65398-5

[28] **Chen M., Lu W., Yan P.**, et al., 2016
Blasting excavation induced damage of surrounding rock masses in deep-buried tunnels, KSCE Journal of Civil Engineering. https://doi.org/10.1007/s12205-015-0480-3

[29] **Hosseini M., Khandelwal M.**, Lotfi R., et al., 2023
Sensitivity analysis on blast design parameters to improve bench blasting outcomes using the Taguchi method, Geomech. Geophys. Geo-Energ. Geo-Resour. https://doi.org/10.1007/s40948-023-00540-4

[30] **Chamanzad M., Nikkhah M.**, 2020
Sensitivity analysis of stress and cracking in rock mass blasting using numerical modelling, Journal of Mining and Environment. https://doi.org/10.22044/jme.2020.10033.1939